2024 10th IEEE RAS/EMBS International Conference for
Biomedical Robotics and Biomechatronics (BioRob)
1-4 September 2024. Heidelberg, Germany

Effects of knee joint misalignments on human-exoskeleton interaction dynamics

Stefano Massardi[1,2], David Rodriguez-Cianca[1], Juan C. Moreno[1], Matteo Lancini[3], and Diego Torricelli[1]

***Abstract*— One aspect that characterizes exoskeletons is their close physical contact with the user. Physical human-exoskeleton interaction (pHEI) is strongly affected by kinematic incompatibilities generated in the human-exoskeleton kinematic chain, often resulting in undesired joint misalignments and interaction forces. However, a systematic analysis to highlight this relation is difficult to execute. In this work we use a methodology for the study of pHEI based on an active dummy leg named Leg Replica. Thanks to this system, our aim is to highlight the relations between key pHEI metrics such as joint misalignment, interaction forces and relative displacements, underlining the role and effects of joint misalignment in controlled conditions. We first validated a kinematic model available in the literature relating human-exoskeleton knee misalignment with the resulting device's motion relative to the limb. The model was further used to investigate which is the relation between the kinematic of the leg-device system and the forces produced between the two bodies. We discovered that the model predictions were consistent with the experimental kinematic observations and strongly related with the peaks reached by shear forces during the motion. Shear forces were found to play a key role in the overall interaction and related with the lost of energy during the motion. These results underscore the strong influence that misalignments can exert on the generation of force and motion, even under simplified and controlled conditions.**

I. INTRODUCTION

Exoskeletons and exosuits are wearable devices that enable, assist, or enhance physical activity through mechanical interaction with the body. In the last decade, many solutions characterized by a multitude of functional goals and target users have moved out of the labs [1][2]. This diversity covers the device type (e.g., lower limb, upper limb, back support), the application domain (e.g., medical, military, industry, consumer), and the functional purpose (rehabilitation, assistance, augmentation) [3]. Independently from their use, a key point in the development of exoskeletons is the human-device coupling and the resulting interaction forces. How to efficiently and safely transmit assistive forces to the human body is still an open issue [4].

In a recent review we highlighted how interaction forces and relative motions between the exoskeleton and the human limbs are strongly related to each other, being crucial aspects of physical human-exoskeleton interaction (pHEI) [5]. The kinematic mismatch between the human and the device causes shear forces to the skin which can in turn compromise safety and comfort [6]. Nevertheless, only a few studies have considered the shear forces contribution to the interaction [7], [8], [9]. The possible relationship between the generation of such shear forces and relative motions may represent an important factor in human-device contact analysis, especially when considering that shear stresses and misalignments can reduce up to 50% of the power transmitted by the exoskeleton to the body [10]. The rigid structure of the exoskeleton creates kinematic restrictions that produce unwanted forces and movements [11]. This structure is often simplified and does not match the user's anatomy, especially when the joints are modeled as single hinge with 1 DoF [12] , while human joints are more complex.On the other side, mimicking the full joint kinematics can lead to bulky and complex devices, which imposes technical limitations.A direct consequence of this oversimplifications is the appearance of human-exoskeleton joint misalignments, which are offsets between the centers of rotation of two bodies that are mechanically connected, and they are a direct consequence of this joint simplification. They can be originated from the initial joints' alignment phase when the device is worn, or due to device's drifts over the body.

The existing literature does not provide a comprehensive analysis of the interrelationships among pHEI metrics [5]. The reason for this lack might be linked to the challenge of i) conducting systematic analyses with human subjects, e.g. test the system in controlled conditions and ii) establishing an instrumental setup capable of extracting the relevant metrics. Specifically, quantifying interaction forces remains challenging unless proper force measurement is introduced at each physical interface [13]. Alternatively, pHEI modeling often employs springs [14] or spring-damper [7], [8] elements to represent human-device contact. A suitable instrumented setup is needed to validate dynamic models of pHEI. Relative displacements can be measured using geometric models that describe how the device's interface moves along the human limb when the joint angles change under different misalignment conditions. However, we do not know how accurate these models are in the real world. Furthermore, the actual impact of joint misalignment can be often partially masked by other variables that can change during the task in a non controlled way.

The goal of this study is to understand this underexplored area by studying how a geometrical model can capture aspects of the contact kinematics and how well its formulation can be extended to a 3D replica of a human leg. After this step, this study wants to link these results with pHEI

[1]S.M, ,D.R.C., J.C.M. and D.T. are with the BioRobotics group, Centre for Automation and Robotics (CAR), Madrid, Spain corresponding author: david.rodriguez.cianca@csic.es

[2]S.M is with the Department of Industrial and Mechanical Engineering (DIMI), University of Brescia, Brescia, Italy

[3]M.L. is with the Department of Medical and Surgical Specialties, Radiological Sciences and Public Health (DSMC), University of Brescia, Brescia, Italy

dynamics and more clearly show how a change in joint misalignment can affect the pHEI dynamics.

We selected a kinematic model from the literature to test whether a mathematical formulation can accurately represent real the limb-device kinematics. The model describes how, under different joint misalignment configurations, a change in angle can lead to a tangential drift of the device's interface along the human limb. The selected model, by Schiele et al. [15], predicts cuff's displacement from joint misalignments while varying the limb angle. The model was originally used to support a dynamic pHEI modelling achieved through an optimization-based parameters identification [15]. However, force and kinematic data were never collected simultaneously. We overcome this limitation by using a method based on an innovative active-sensing dummy leg for pHEI measurement, named Leg Replica [16]. The Leg Replica was already tested for a systematic pHEI analysis and able to prove the effect of a misalignment compensation mechanism on interaction forces [17]. With this analysis we want to assess to which extend a planar kinematic model can account for real 3D shapes, that are not represented in the model. This is achieved by comparing the observed relative motion with the predictions made by the model. This work wants, first, to verify through an experimental session the theoretical relation between joint misalignments and relative motion proposed by the aforementioned model.

Secondly, we aim to understand the relation between the model's prediction and real interaction forces. Thanks to a simplified and controlled setup, we can manipulate joint misalignment in a controlled environment. This allowed us to more clearly highlight the effect of a change in joint misalignment on the generation of shear forces.

II. MATERIALS AND METHODS

This work is structured on two analysis named *Kinematic analysis* tests and *Dynamic analysis* tests. In the *Kinematic analysis tests*, we want to assess the kinematic model formulation with respect to experimental relative motion data. This analysis did not include any force measurement and is based on kinematic metrics such as relative motions and joint misalignment. In the *Dynamic analysis tests* we introduced interaction force measurement to clarify the relations between dynamic and kinematic pHEI metrics and focus on the dynamic effect of a change in joint misalignment.

A. Kinematic Model of Misalignments

The work presented in [15] describes a mechanical model of single degree of freedom interaction between a human joint and a wearable robot. The model is used to predict the constraint displacements *d* that exist between the limb and the robot if their centre of rotations have offsets M_X and M_Y. Although the model was developed for an upper arm exoskeleton, the same formulation can be applied for a lower limb. The characters used in the model are here reported in accordance with [15] and conventions in Fig. 1.

- α: knee joint angle
- β: orthosis angle
- γ: angle misalignment in XY plane (around z-axis)
- M_x,M_y: X,Y knee misalignment (along x and y-axis)
- z_{ex}: link offset around the distal attachment point (35 mm)
- l_{ex}: fixed distance from marker LS1 to marker OC (132 mm, see Section II-E)

According to the model, the total predicted cuff displacement along the human segment (*d*) is described by the difference of a linear and rotational component $d = d_{lin} - d_{rot}$ where $d_{lin} = l_{const} - l_{var}$ and $d_{rot} = tg(\gamma) \cdot z_{ex}$. To obtain a cuff displacement relative to the initial position, the factor l_{const} can be set to zero while l_{var} formulated as:

$$l_{var} = \sqrt{c^2 + l_{ex}^2 - 2 \cdot c \cdot l_{ex}^2 \cdot cos(\epsilon)} \tag{1}$$

with $c = \sqrt{M_x + M_y}$ and $\epsilon = \pi - \arctan(M_y/M_x) - \beta$. For the rotational component (d_{rot}), angle γ is computed as function of β:

$$\gamma = \arcsin \frac{c \cdot \sin(\epsilon)}{c^2 + l_{ex}^2 + 2 \cdot c \cdot l_{ex}^2 \cdot cos(\epsilon)} \tag{2}$$

B. Passive knee orthosis

The kinematic model is based on the ideal assumption that a 1-DOF device can freely slide over two human segments connected by an ideal hinge joint. To get close to this condition and remove other bias effects, we selected a passive light wearable device with a negligible friction at the knee joint. It consists of a commercially available knee orthosis (REAQER Orthosis) composed by 2 light aluminium frames connected by a hinge joint. Each frame has two cuffs for the fixation on the leg. To ensure that the model's conditions are replicated, any relative motions between the orthosis and the Leg Replica's thigh have been prevented.

C. Leg Replica

The tests of this work were conducted on a dummy leg called Leg Replica, designed to replicate the shape, dimensions, weight, inertia, and motion of a real human leg [16]. The Leg Replica is equipped with 8 triaxial load cells located beneath its external surface, 4 in the shank and 4 in the thigh, allowing a clean wearing of a wearable device. Its external surface is composed by 3D-printed shells made of ABS material. Both the thigh and shank segments include four 3D-printed surface shells (Fig. 2c), two at the front side and two at the back side. Each shell is connected to the corresponding load cell, which allows to detect interactions along three axes. The knee joint is an actuated hinge that enables the position control of the articulation. Hip and ankle are passive ball joints that can be blocked in a predefined position. This innovative device enables high repeatability and control of the conditions, which is normally difficult to achieve in humans. The simplified knee joint mechanism, together with the use of a light passive orthosis, can favour the replication of the ideal geometric condition considered by the model and depicted in Fig. 1a. A marker-based vision system

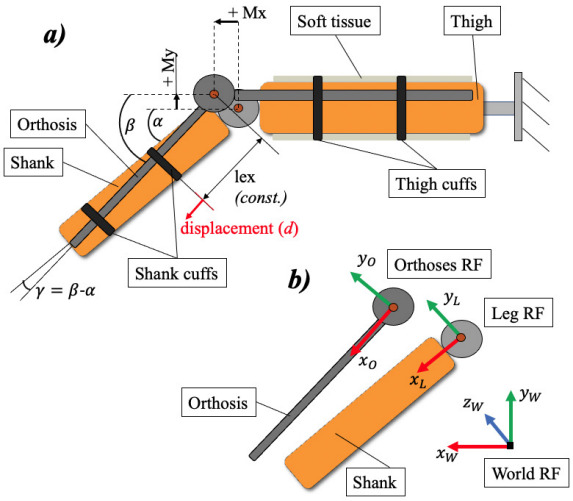

Fig. 1: Scheme of the Leg Replica coupled with the orthosis, showing a) symbol and sign convention in accordance with the selected kinematic model and (b) the reference frames (RFs) for all the trials

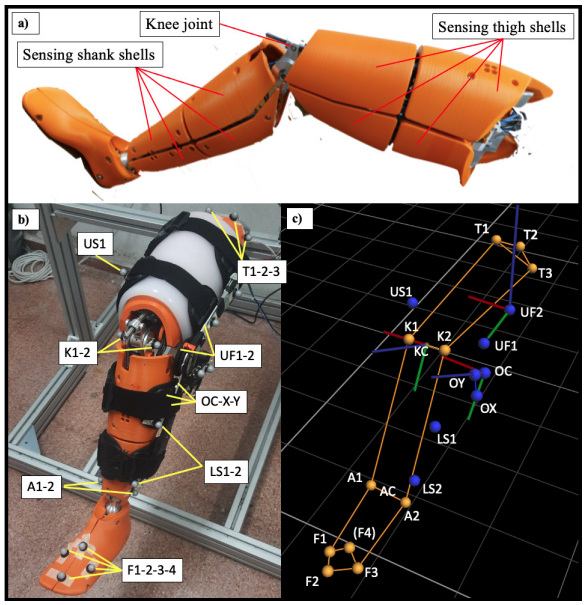

Fig. 2: Leg replica view and marker protocol. (a) Lateral view of the Leg-Replica prototype and its sensing surface shells. (b) Knee orthosis attached to the Leg-Replica prototype, including reflective markers by name. The silicon layer is visible on the thigh segment (white material). (c) Leg-replica's VICON model with markers name and the computed reference systems for the leg knee and the exoskeleton knee. Markers are placed on the thigh cuff (UL1), upper device frame (UF1,UF2), shank cuffs (LS1,LS2), orthosis knee frame (OC,OX,OY), leg thigh (T1,T2,T3), leg knee hinge (K1,K2), leg ankle (A1,A2) and foot (F1,F2,F3,F4).

composed of 8 IR VICON Vero cameras (VICON, Oxford, UK) is placed around the Leg Replica for the extraction of kinematic metrics. A silicon layer (EcoFlex 00-30, Smooth-On) is placed on the Leg Replica's thigh to increase friction and allow a better fastening of the orthosis, and consequently favour the motion along the shank in accordance with the model formulation. No comprehensive skin formulations were considered for the purpose of simplification.

D. Experimental protocol

We conducted two different analyses: i)*kinematic* analysis focusing on the experimental validation of the kinematic model and ii)*dynamic* analysis assessing the relationship between the model predictions, joint misalignment and interaction forces recorded by the Leg Replica.

The preparation of the setup was common to all the trials. The Leg Replica hip was attached to an horizontal bar and blocked with the thigh parallel to the ground. Nineteen reflective markers were used for the protocol (11 placed on the Leg Replica and 8 on the orthosis), as shown in Fig. 2, following the protocol described in Section II-E. The knee joint was blocked at 0^o (fully extended leg) and markers' position recorded. This preliminary step allowed to verify the residual angle between the knee reference frame (RF) and the world RF (RFs described in Section II-E). This procedure ensured the leg parallel to the ground along the 3 axis. The ankle ball joint was also blocked in a non-predefined position, since this parameter doesn't affect the measurements. Afterwards, the orthosis was mounted onto the Leg-Replica. The remaining reflective markers were then placed on the orthosis, following the protocol depicted in Fig. 2 and Section II-E.

1) Kinematic analysis tests: This analysis aimed to prove the reliability of the model across different misalignment configurations in the XY space. To replicate the ideal model conditions, the orthosis cuff must be free to slide along the shank segment. For this analysis, the silicon layer was attached on the thigh segment only. The orthosis thigh cuffs were strongly fastened around the thigh so that no significant relative motions could be transmitted on this segment. Avoiding this motion is of key importance to replicate the ideal condition considered by the model, where the motion is entirely transmitted to the shank cuffs. For the same reason, the shank cuffs were fastened with very low strapping forces to enable the sliding motion along the x-axis with negligible interaction forces. For each test, the orthosis was manually positioned to reach a different misalignment condition along the x and y-axis, according to the convention in Fig. 1. The relative angle between leg and orthosis in the sagittal plane (angle γ in Fig. 1a) was not controlled during the alignment phase. The reached condition was roughly checked with a meter, whereas a more accurate misalignment quantification was computed in the post processing phase. The thigh cuffs were well fastened to block the configuration before actuating the Leg Replica. We considered that a manual alignment phase could only achieve a position accuracy of 10 mm. For this reason, a configuration with a knee joint misalignment of less than 10 mm with respect to the leg's joint was considered aligned, and named as neutral misalignment condition. For this analysis, we imposed eleven

different misalignment conditions along the x and y-axis (Fig 3a). The leg was commanded to follow a sinusoidal position reference in the range 5-65deg with a frequency of 0.2Hz.

2) Dynamic analysis tests: For the dynamic analysis tests all the orthosis cuffs were fastened tightly to the leg. The silicon layer was added on both thigh and shank to produce significant interaction forces and prevent unrealistic relative motions. To make the runs comparable, similar initial strapping forces were guaranteed for the same cuff across the runs. Strapping forces were checked at the beginning of the test for each load cells' axis of the LegReplica, making sure that each single force component did not differ more than $\pm$10N between the trials. Thirteen misalignment conditions were imposed in the XY plane to test the consistency of the force-displacement relation. The imposed misalignment conditions were achieved by simulating incorrect device mounting, but avoiding scenarios where the misalignment would be unrealistically extreme due to the excessive effort required to induce it. The same trajectory used in the *kinematic analysis* was used to command the leg.

E. Marker Placement and VICON Model

In order to measure misalignments and relative motions between the leg and the orthosis, we used a reflective marker setting (VICON Vero). The marker placement is presented in Fig. 2b and 2c. Two virtual markers for the ankle center (AC) and knee center (KC) were computed as the middle point of the segment A1A2 and K1K2 respectively. The KRF was computed with origin in KC, x-axis along KCAC, z-axis as KCK1 and y-axis as product of the two. The orthosis reference frame (ORF) was computed by placing a 3D printed orthogonal cluster directly on its joint with the marker OC aligned with the orthosis center of rotation and OX and OY along the x and y directions, in accordance with the KRF. Since the marker K1,K2,A1 and A2 are crucial for the RFs computation, they were reconstructed in the post processing phase to avoid marker occlusions that normally happen during the leg motion. The position of the knee markers K1 and K2 was reconstructed with respect to a fixed RF built from T1,T2,T3 on the thigh, while the ankle markers relative position was calculated from a fixed RF on the foot (F1, F2, F3). Markers US1 and LS1 were placed for the extraction of the cuff's relative motions. Marker LS2 was placed to replace marker LS1 in case of problematic marker occlusions.

F. Metrics

The main metrics considered in our analysis are:

- Spatial misalignment (M_x,M_y): x-y offset between the position of marker KC and marker OC.
- Relative cuff displacement relative to the shank (*d*): position of the marker LS1 along the x-axis of KRF. The model refers to this metric.
- Relative cuff displacement relative to the thigh: position of the marker US1 along the x-axis of the WRF.
- Resultant force (shank/thigh): Vector sum of the 3 force components. The metric considers the sum of resultant forces from the sensors in the shank/thigh segment.
- Shear force (shank/thigh): interaction force component along the x-axis of the segment considered (KRF for the shank, WRF for the thigh). The metric shank/thigh shear force considers the sum of shear forces from the sensors in the shank/thigh segment.
- Energy loss: Energy lost during the motion due to the device's sliding and rubbing over the leg. Computed as the cumulate of $F_s \cdot d$ for each sample, where F_s is the shear force for each sensor and d the relative cuff's displacement.

Model's prediction accuracy was assessed through the root mean squared error (RMSE) between the measured relative cuff displacement (*d*) and the model prediction. An estimation of the uncertainty was carried out on all metrics to enable further considerations and check the validity of the final results. Cameras were calibrated before every session following the standard VICON calibration procedure. The single marker position's uncertainty was declared by the software. This uncertainty is propagated in the computations needed to compute the metrics. A Monte Carlo method was applied to the data from a real test, where each marker's coordinate was perturbed 1000 times per frame along a normal distribution with σ taken as the highest marker uncertainty declared by the software after the standard VICON calibration procedure (σ=0.2 mm).

III. RESULTS

A. Metrics uncertainty

The calculated uncertainty associated with the VICON metrics along the three axes is collected in Table I.

TABLE I: Metrics uncertainty

Metric	**x-axis**	**y-axis**	**z-axis**
Angle knee misalignment γ [deg]	0.8	2.7	2.7
Spacial knee misalignment M_x, M_y, zex [mm]	0.8	0.6	0.5
Cuff's relative displacement d [mm]	1.7	2.1	2.0

B. Kinematic analysis tests

Figure 3a shows the 11 misalignment conditions reached in the misalignment analysis that gradually covered the x-axis and part of the y-axis. Figure 3b presents the accuracy of the model in predicting the relative motion between the leg and the device. Predictions were consistently scoring similar RMSEs values across all the trials (1.3 $\pm$0.7 mm), with higher relative errors when the experimental motion was reduced. Experimental measured motion was limited in conditions where orthosis knee was closer to the leg knee rotation center although not symmetrically along the axis. Fig. 4 a-b) highlights two examples of relative motions as a function of knee movement phase for conditions 1.7 and 1.11. The model was able to predict intensity, sign and shape of the experimental motion.

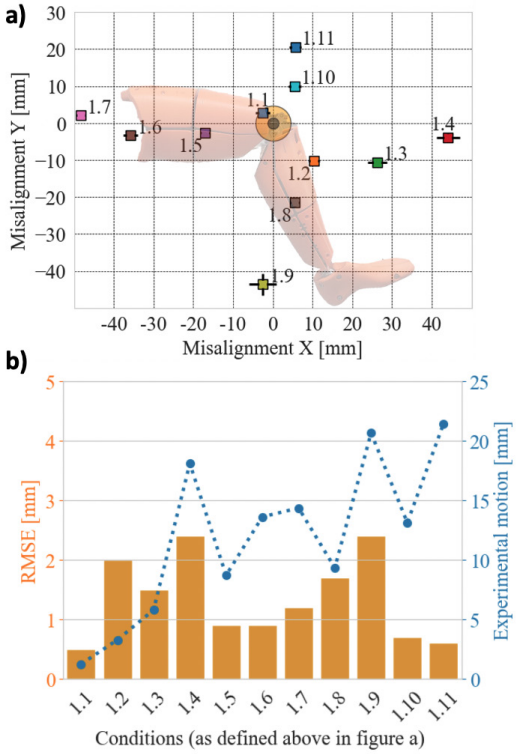

Fig. 3: Conditions and results of kinematic analysis. a) XY misalignment conditions reached in the kinematic analysis. Markers' coordinates represent the initial misalignment of the orthosis joint with respect to the leg's knee joint that is here centered in the origin [0,0], (shaded leg is not scaled). The cross on each marker represents the standard deviation of the recorded misalignment during each trial in x and y direction. A progressive number is assigned to identify each run. b) RMSE (orange bars) in mm (left y-axis) obtained between measured relative motion and model prediction for each of the conditions in figure a). Blue dotted line represents the range of motion of the real shank cuff's displacement in mm (right y-axis) recorded in each condition.

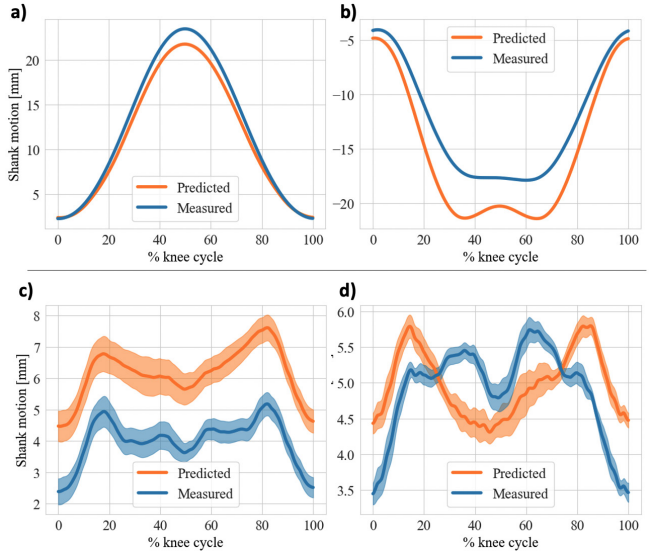

Fig. 4: Measured (blue lines) and predicted (orange lines) cuff's relative motions segmented on the knee cycle. A knee cycle consists of a motion from 65^o (knee flexed) to 5^o (knee extended) and back to knee flexed position. The plots show examples from condition 1.7 (a) and condition 1.11 (b) from the kinematic analysis, and condition 2.4 (c) and condition 2.11 (d) from the dynamic analysis

C. Dynamic analysis tests

Misalignment configurations showed higher standard deviations compared to the previous analysis, as shown in Fig. 5a. Fig. 5b shows error values consistent with Fig. 3b with RMSE 1$\pm$0.8 mm. Experimental relative motion was also very limited at the shank level when compared to the kinematic analysis. Higher displacement was observed at the thigh interface (red line, Fig. 5b) when the center of rotation of the orthosis was closer to the thigh (from conditions 2.7 to 2.13). For the remaining conditions, with the orthosis center closer to the shank, the motion mainly occurred along the shank (blue line, Fig. 5b), although limited.

Shear forces can be represented as a percentage of the total resultant force recorded from all three axes in each condition. This proportional contribution is illustrated in Fig. 6, with each condition represented on its initial misalignment XY coordinate (as in Fig 5a) together with the weight in % on the resultant interaction. Shear forces could range between 32% and 59% of the resultant force and on average occupied the 47% of the interaction. For conditions with misalignment towards the hip (negative x-axis), shear component averagely weighted 55% of the resultant force.

The greater relative displacements of the orthosis' cuff in the thigh, as opposed to the shank, suggest a more rigid connection of the orthosis in the shank. This is contrary to the conditions examined during the kinematic analysis tests, where the orthosis was securely fastened to the thigh and had freedom of movement at the shank. Despite this, the model's formulation is still applicable. Fig. 7a illustrates the relative motion predicted by the model, related with the shear forces recorded in the two leg segments (shank/thigh). The findings underscore a robust correlation (intra-class correlation, ICC) with the shear forces recorded at the thigh (ICC:0.89) and the shank (ICC:0.85) segment. This information can be summarized in Fig. 7b, depicting a color map computed with the total relative displacement predicted by the model for a 60^o motion of the knee as a function of the initial human-exoskeleton joint misalignment in the XY plane. The graphic overlays the maximum shear force recorded at the shank level (grey shaded dots) in the misalignment conditions displayed in Fig. 5b). As observed in general, experimental shear force values relate with the model predictions, i.e. higher cumulative predicted motions are consistent with the experimentally obtained higher shear forces, whereas for misalignment conditions where lower motion is predicted, results present lower shear forces.

The energy loss resulting from the orthosis's displacement

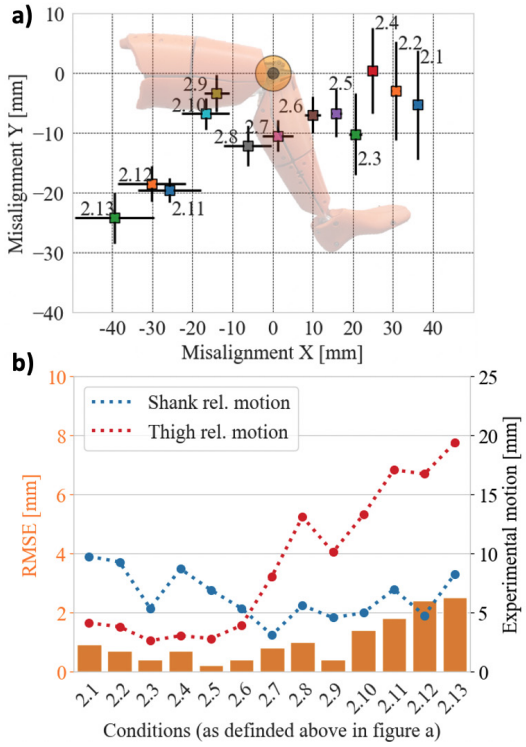

Fig. 5: Conditions and results of dynamic analysis. a) XY misalignment conditions reached in the dynamic analysis session. Markers' coordinates represent the initial misalignment of the orthosis joint with respect to the leg knee joint that is here centered in the origin [0,0], (shaded leg is not scaled). The cross on each marker represents the standard deviation of the recorded misalignment during the trial in x and y. A progressive number is assigned to identify each run. b) RMSE (orange bars) in mm (left y-axis) obtained between measured relative motion and model prediction for each of the above conditions. Blue and red dotted line respectively represent the range of motion of the shank and thigh cuff's displacement in mm (right y-axis) recorded in each condition

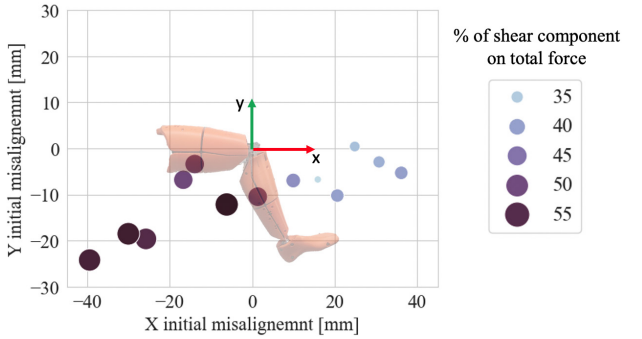

Fig. 6: % Contribution of shear component on the total resultant force for each condition of the dynamic analysis. The size of the markers in the plot corresponds to the magnitude of the percentage of shear component on the total resultant force, and their position represents the initial misalignment condition in the XY plane (as shown in Fig. 5a). The leg is depicted for reference, with the knee positioned at the origin [0,0] (not scaled).

relative to the leg was quantified for each condition. This was determined by the total energy lost due to shear forces acting on the relative displacement during movement. Fig. 8 presents the results, with each condition represented on its initial misalignment XY coordinate together with the energy in the motion. Energy loss could vary between 3.8J and 19.5J, solely as a result of a change in misalignment. To underline the variations among conditions, the energy loss is expressed as a percentage of a reference condition, which is selected as the one nearest to the XY origin of perfect alignment between the leg and the device. Scenarios with a negative X misalignment dissipated up to 3.5 times the energy of the reference. Differently, trials with a positive X alignment had comparable or lower energy levels.

IV. DISCUSSION

One of the Leg Replica's advantages is its potential to serve as platform to systematically study pHEI and conduct preliminary experiments in controlled conditions. Our setup enabled us to conduct tests in semi-ideal conditions, where we could control the effects of changes in a single parameter. This allowed us to maintain consistent test conditions, with the only variable being joint misalignment. As a result, we were able to more clearly highlight the net effect of misalignment. The first part of this work was so called "kinematic analysis". This phase was not supposed to relate to a real-life situation but rather to conduct a validation of a kinematic-based interaction model, by measuring joint misalignments, relative motions and interaction forces in a real leg-device system. The geometry-based model had not been previously tested for its accuracy using kinetic and kinematic metrics in a realistic scenario. The model consists of 2D mass-free linear links and was tested on a 3D shaped leg with mass and inertia comparable to a real human leg. Nonetheless, we demonstrated that the model could accurately predict the real relative motion of the of the orthosis' cuff with respect to the leg for multiple initial misalignment conditions.

The dynamic analysis sessions focused on the relation between interaction forces and relative motions. Fig. 7a showed how the model prediction could represent a general indicator of shear forces generated on the leg due to joint misalignment. The result highlighted that the contact could be linearly approximated. During the experiments, it was observed that the relative movements at the thigh segment were more pronounced. However, this was only evident when the center of the orthosis joint was shifted towards the thigh. On the other side, a misalignment that moved the orthosis towards the shank resulted in fewer relative movements, which were more pronounced at the shank segment. This interaction effect at the thigh is consistent with existing literature, which asserts that "knee misalignment significantly changes interaction forces, especially at the thigh interface," and that this change is more noticeable for misalignments

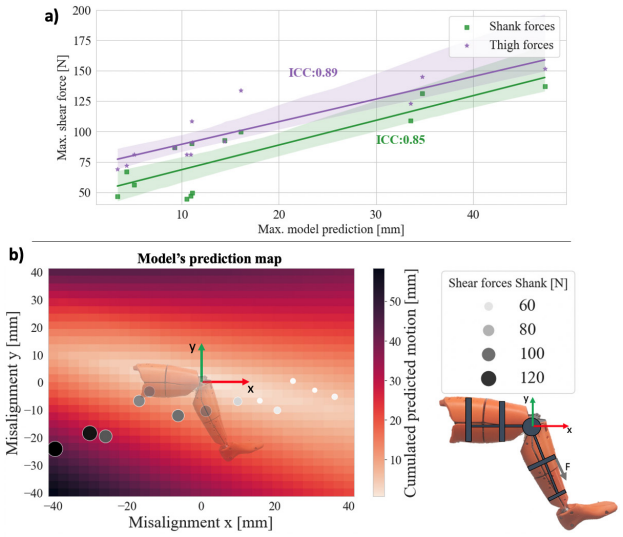

Fig. 7: Relations between the metrics of the dynamic analysis. a) Range of relative motion predicted by the model related with maximum shear forces recorded in thigh and shank. Shaded areas refers to a 95% confidence interval. ICC value represent the intra-class correlation score between the two metrics. b) Intensity-based colormap built from the model equation in the XY misalignment space. The map intensity refers to the cumulative motion predicted for a knee angle from 0^o to 65^o. Maximum shear forces at the shank are overlaid on the map placed at the XY coordinate of the initial misalignment condition for each trial (as Fig. 5a) and colored on a different intensity palette. The leg is shaded as reference with the knee placed in the origin [0,0] (not scaled).

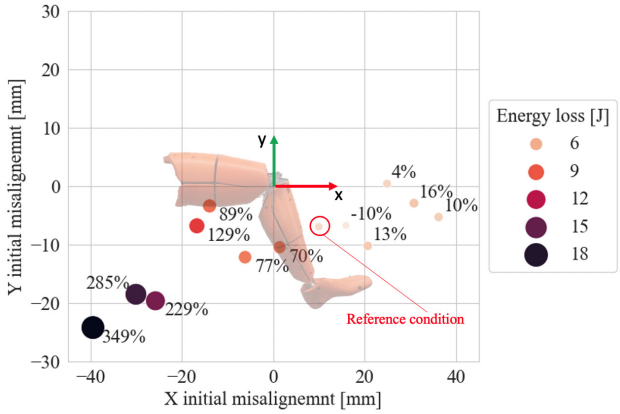

Fig. 8: Energy loss for each condition of the dynamic analysis. The size of the markers in the plot corresponds to the magnitude of the energy loss, and their position represents the initial misalignment condition in the XY plane (as shown in Fig. 5a). The relative energy loss for each trial is calculated as a percentage of the energy lost in a reference condition. The reference condition is selected as the XY misalignment condition that is nearest to the origin (0,0). The relative energy is displayed next to each marker in percentage terms. The leg is depicted for reference, with the knee positioned at the origin [0,0] (not scaled).

towards the hip [13]. Despite the model considered the cuff fixed at the thigh and movable along the shank, and our experiments generally showed an opposed condition, model's predictions were also valid given the symmetry of the model. This is shown by the high correlation obtained between the model prediction and the measured forces (Fig. 7a). Although the misalignment was changing during the motion, the result proves the strong interconnection between the considered metrics and the initial misalignments configuration. The model's results also suggests that a prediction based purely on kinematics can provide a global understanding of the system's efficiency and dynamic behavior under various misalignment conditions. The model can map the XY misalignment plane, identifying areas subject of less relative motions and consequently lower undesired interaction forces (Fig. 7b). This mathematical relationship between kinematic metrics and forces is crucial for understanding pHEI and for the development of future interaction models. Validating this map through a larger number of experimental conditions and strapping forces could help clarify the impact of different misalignment components on the system motions and further demonstrate the model's consistency. A significant result of this study is that a minor change in misalignment, even when dealing with a lightweight orthosis device, can have an important impact on the generation of shear forces. Shear forces represent a crucial measure of the efficiency of force transmission in an exoskeleton. Our tests revealed that the shear force component could make up to 59% of the total interaction force and on average, constituting 47% of the overall force. This energy loss comes as friction on the user's body and leads to a reduction of the motion efficiency transmission. These results show the need to consider and monitor this metric in future safety assessments of exoskeletons. We observed how the single misalignment effect could amplify energy dissipation by up to 3.5 times compared to more aligned conditions. These outcomes are significant, especially considering that our tests were conducted with a lightweight device, with minimal joint friction, and under controlled conditions. In a real-world human-exoskeleton scenario, the single impact of misalignment could potentially have even more severe implications. These insights are particularly crucial when considering that the international community is still in the process of developing a clear method for exoskeleton safety assessment [18]. One significant insight from this study is the inherent challenge in manually achieving a desired misalignment. Considering the controlled setup, in some conditions we aimed to achieve a purely zero human-exoskeleton misalignment. However, a perfect knee joint alignment was difficult to achieve (Fig. 3a and 5a), as we could only reach alignments close to 10 mm. This implies that, in practice, achieving perfect alignment between exoskeletons and human joints will be challenging due to the intrinsic complexity of joints, the presence of soft

tissues, and the difficulty of the procedure.

This work presents a series of limitations. The difficulty in alignment, coupled with the need to maintain similar strapping forces across trials, hindered a full control of the orthosis position during the dynamic analysis. As a result, not all possible misalignments in the XY plane were covered, leaving some unexplored areas. Despite this, the results can still be seen as a random scan of the XY plane, demonstrating a general consistency with the predictions. While a device equipped with a sliding component could have led to more accurate results, we tried to minimize friction forces in the kinematic analysis as much as possible. Despite these considerations, the consistent results obtained from the model formulation suggest that the impact of the device and other non-ideal factors was relatively limited.

Another important point concerns the lack of comparison with human experiments. We believe that to validate the consistency of the results and estimate the applicability of the proposed methodology, experiments involving humans will also need to be conducted. However, we also believe that human involvement should be included in a separate study as it requires modifications to the experimental protocol presented here. The difficulty to apply pHEI measurement on humans is what makes it a poorly explored field. The proposed setup and methodology brings advantages to the field as it allows to conduct systematic experiments to obtain basic scientific knowledge and evidence to guide human-based research on pHEI.

V. CONCLUSIONS

With the help of a mechatronic Leg Replica we were able to experimentally assess the effects of different knee misalignments on the relative motion between a passive orthosis and a human-like leg. In particular, we tested the validity of an existing kinematic model, and explored the ability of the model predictions to inform about the force transmission. The model showed high consistency in predicting the motion under different knee misalignment conditions. The model predictions could map the motion of the kinematic limb-device configuration with the measured interaction forces, in particular with the shear forces generated during the motion. These forces were found to be key metrics in terms of contribution to the overall interaction, energy dissipation and relation with kinematic incompatibility. Thanks to the proposed setup, we could extract meaningful evidence on the physical interaction dynamics between an exoskeleton and the human leg. Considering the limited research on the topic, we believe that any attempt to explore an area such as pHEI would be a valuable contribution to the community and could serve as a helpful guide for the future directions.

ACKNOWLEDGMENT

This work was supported by the project EXOSAFE, awarded by the COVR European Project under grant agreement No. 779966.

REFERENCES

[1] R. Bogue, "Exoskeletons–a review of industrial applications," *Industrial Robot: An International Journal*, 2018.

[2] R. Gopura, D. Bandara, K. Kiguchi, and G. K. Mann, "Developments in hardware systems of active upper-limb exoskeleton robots: A review," *Robotics and Autonomous Systems*, vol. 75, pp. 203–220, 2016.

[3] W. Huo, S. Mohammed, J. C. Moreno, and Y. Amirat, "Lower limb wearable robots for assistance and rehabilitation: A state of the art," *IEEE systems Journal*, vol. 10, no. 3, pp. 1068–1081, 2014.

[4] J. Damerau, J. Jovic, T. Watanabe, and U. Wolz, "On the effect of attachment position and compliance of wearable robots on human joint and interface forces," 2015.

[5] S. Massardi, D. Rodriguez-Cianca, D. Pinto-Fernandez, J. C. Moreno, M. Lancini, and D. Torricelli, "Characterization and evaluation of human–exoskeleton interaction dynamics: A review," *Sensors (Basel, Switzerland)*, vol. 22, no. 11, 2022.

[6] X. Mao, Y. Yamada, Y. Akiyama, S. Okamoto, and K. Yoshida, "Safety verification method for preventing friction blisters during utilization of physical assistant robots," *Advanced Robotics*, vol. 31, no. 13, pp. 680–694, 2017.

[7] K. Langlois, D. Rodriguez-Cianca, B. Serrien, J. De Winter, T. Verstraten, C. Rodriguez-Guerrero, B. Vanderborght, and D. Lefeber, "Investigating the effects of strapping pressure on human-robot interface dynamics using a soft robotic cuff," *IEEE Transactions on Medical Robotics and Bionics*, vol. 3, no. 1, pp. 146–155, 2020.

[8] Y. Akiyama, Y. Yamada, and S. Okamoto, "Interaction forces beneath cuffs of physical assistant robots and their motion-based estimation," *Advanced Robotics*, vol. 29, no. 20, pp. 1315–1329, 2015.

[9] X. Wan, Y. Liu, Y. Akiyama, and Y. Yamada, "Monitoring contact behavior during assisted walking with a lower limb exoskeleton," *IEEE transactions on neural systems and rehabilitation engineering*, vol. 28, no. 4, pp. 869–877, 2020.

[10] M. B. Yandell, B. T. Quinlivan, D. Popov, C. Walsh, and K. E. Zelik, "Physical interface dynamics alter how robotic exosuits augment human movement: implications for optimizing wearable assistive devices," *Journal of neuroengineering and rehabilitation*, vol. 14, no. 1, pp. 1–11, 2017.

[11] V. Bartenbach, "Constraints caused by lower extremity exoskeletons," Ph.D. dissertation, ETH Zurich, 2017.

[12] G. Wu, S. Siegler, P. Allard, C. Kirtley, A. Leardini, D. Rosenbaum, M. Whittle, D. D D'Lima, L. Cristofolini, H. Witte, *et al.*, "Isb recommendation on definitions of joint coordinate system of various joints for the reporting of human joint motion—part i: ankle, hip, and spine," *Journal of biomechanics*, vol. 35, no. 4, pp. 543–548, 2002.

[13] D. Zanotto, Y. Akiyama, P. Stegall, and S. K. Agrawal, "Knee joint misalignment in exoskeletons for the lower extremities: Effects on user's gait," *IEEE Transactions on Robotics*, vol. 31, no. 4, pp. 978–987, 2015.

[14] A. Schiele and F. C. Van der Helm, "Influence of attachment pressure and kinematic configuration on phri with wearable robots," *Applied Bionics and Biomechanics*, vol. 6, no. 2, pp. 157–173, 2009.

[15] A. Schiele, "An explicit model to predict and interpret constraint force creation in phri with exoskeletons," in *2008 IEEE International Conference on Robotics and Automation*. IEEE, 2008, pp. 1324–1330.

[16] M. Dežman, S. Massardi, D. Pinto-Fernandez, V. Grosu, C. Rodriguez-Guerrero, J. Babič, and D. Torricelli, "A mechatronic leg replica to benchmark human–exoskeleton physical interactions," *Bioinspiration & Biomimetics*, vol. 18, no. 3, p. 036009, 2023.

[17] S. Massardi, D. Rodriguez-Cianca, M. Cenciarini, D. C. Costa, J. M. Font-Llagunes, J. C. Moreno, M. Lancini, and D. Torricelli, "Systematic evaluation of a knee exoskeleton misalignment compensation mechanism using a robotic dummy leg," in *IEEE... International Conference on Rehabilitation Robotics:[proceedings]*, vol. 2023, 2023, pp. 1–6.

[18] S. Massardi, D. Pinto-Fernandez, J. F. Veneman, and D. Torricelli, "Testing safety of lower limbs exoskeletons: current regulatory gaps," in *Wearable Robotics: Challenges and Trends: Proceedings of the 5th International Symposium on Wearable Robotics, WeRob2020, and of WearRAcon Europe 2020, October 13–16, 2020*. Springer, 2022, pp. 145–149.